Available online at www.sciencedirect.com
ScienceDirect
Publishing Services by Elsevier
International Journal of Naval Architecture and Ocean Engineering xx (2016) 1–11
http://www.journals.elsevier.com/international-journal-of-naval-architecture-and-ocean-engineering/

# Study of a vibrating propulsion system for marine vessels: Evaluation of the efficiency for a boat 13 m long

Roberto Muscia

*Department of Engineering and Architecture, University of Trieste, Piazzale Europa n. 1, 34127 Trieste, Italy*

Received 9 June 2016; accepted 26 September 2016
Available online ■ ■ ■

**Abstract**

This paper illustrates recent advancements relative to a non-conventional propulsion system for boats and is based on two previous papers of the author presented at a conference (see Muscia, 2015a,b). The system does not consider propellers and utilizes the vibration generated by two or more pairs of counter rotating masses. The resultant of the centrifugal forces applies an alternate thrust to the hull that oscillates forward and backward along the longitudinal axis of the boat. The different hydrodynamic drag forces that oppose to the oscillation produce a prevalently forward motion of the vessel. The vibration that causes the motion can be suitably defined to maximize the forward displacement and the efficiency propulsion of the system. This result is obtained by using elliptical gears to rotate the counter rotating masses. The computation of the propulsion efficiency is based on a suitable physical mathematical model. Correlations between numerical experiments on models and possible full scale application are discussed. Some remarks in relation to practical applications and critical issues of the propulsive solution are illustrated. The results have been obtained with reference to a CAD model of a real boat already manufactured whose length is approximately equal to 13 m.


*Keywords:* Naval propulsion; Dynamics; Vibrations; Motion equations; Centrifugal force; CFD computation

## 1. Introduction

The propeller is the most diffuse device for the naval propulsion. Nevertheless, as noted for example in 2006, Muscia and Sciuto, 2010, Muscia, 2015c, by using this device some problems can rise. However, nowadays it is impossible to waive the propellers. Nevertheless, some researchers have performed some studies in order to find possible new alternative propulsion device.

In Guglielmini et al. (2004), Floc'h et al. (2012), Belibassakis and Politis (2013), Esfahani et al. (2015), Xia et al. (2015), some hydrodynamics modelization to study possible fish-like swimming propulsion device are developed. Other operating principles based on oscillating masses have been considered in Chernousko (2002, 2005, 2006, 2008), Fang and Xu (2011, 2012), Shaw (1986), Yang et al. (2013), Li et al. (2005, 2006), Muscia and Sciuto (2010), Muscia (2015c). In these last two papers the authors evaluate if there is a practical possibility of obtaining a rectilinear motion of a body partially or totally submerged without using propellers and fish-like swimming. These two studies are based on a propulsion system consisting of counter rotating masses installed within the hull. The centrifugal force generated by these masses causes a forward displacement of the vessel because the hydrodynamic drag force applied to the vessel is different when it oscillates back and forth due to the centrifugal force. In this regard, the numerical simulations show that it is possible to achieve a significant displacement in the case of small models (vessel models about 1.7 m long) with propulsive efficiency that can be equal to 0.45 or more (Muscia, 2015c). Obviously, in order to offer an engineering solution, an acceptable propulsive efficiency is not the only parameter that has to be considered. However, if the propulsive efficiency is not acceptable it will certainly not be convenient to continue

*E-mail address:* muscia@units.it.
Peer review under responsibility of Society of Naval Architects of Korea.

http://dx.doi.org/10.1016/j.ijnaoe.2016.09.011

with a further study to resolve all the other engineering problems. Therefore, since the results obtained in Muscia and Sciuto (2010), Muscia (2015c) referred to a ship model of which the length is equal to only 1.7 m, in the present study the propulsive efficiency based on counter rotating masses and shaped stern is evaluated with reference to a virtual model in scale 1:1 relative to a real vessel about 13 m long. In order to perform this evaluation, we use the same methodology described in Muscia (2015c). The structural and functional data of the new vessel were provided by Di Ubaldo (2010). In the following Section 2 we illustrate the functioning of the new propulsion system and the corresponding physical mathematical model by which it is possible to evaluate the performance of the system, in particular the propulsive efficiency. Section 3 illustrates and discusses the numerical results obtained with reference to the virtual model of the real vessel about 13 m long.

## 2. Physical mathematical model of the propulsion system

It is well known that the centrifugal force is an apparent force associated with the centripetal force which bends the trajectory of a body. The generation of the centripetal force can be obtained by a constraint. The constraint allows the definition of the apparent force called "centrifugal force". In the specific case of the propulsion system studied we can think that a body totally or partially submerged in a liquid is subject to an action of "partial" constraint represented by the hydrodynamic drag force. The effect of the centrifugal force applied to the above-mentioned constraint generates a reaction force. This force opposes the motion of the body, regardless of the motion direction is. Therefore, in relation to the nature of the body-liquid system, the "liquid" constraint generates a force that, instant by instant, opposes the centrifugal force. However, unlike the situation where the constraint is fixed and the constraint reaction is always equal to the centrifugal force (in the case of constant angular speed), if one considers a vessel, the constraint, whose reaction force is represented by the hydrodynamic drag force, "follows" the motion of the same vessel. Furthermore, this hydrodynamic drag force depends on the shape of the hull and on the direction of the vessel velocity. By suitably shaping the stern and the bow of the vessel, it is possible to minimize and maximize the hydrodynamic drag force when the hull moves forward and backward, respectively. Therefore, the magnitude of the relative speed of the hull with respect to water being the same, the hydrodynamic drag force will be greater when the vessel moves backward. We can consider one or more pairs of counter rotating masses having the same crank radius installed within the vessel. Each pair of masses rotates around two corresponding centres. The relative rotation angles are timed so that the components of the pair of centrifugal forces along a direction perpendicular to the axis of the hull, vanish instant by instant. Conversely, the components along the same axis add up and generate a resultant that changes whenever the crank radii of the two masses move from a horizontal position to a different one. In the instant in which these radii are horizontal, the resultant is equal to zero, afterwards it is not null and is oriented along the direction of the bow or the stern of the vessel, versus the rotation angle relative to the same crank radii. Fig. 1 shows a scheme of the principle of operation previously described by considering, for example, only two pairs of counter rotating masses. In Fig. 1, $F_{id}$, $m$, and $F_c$ represent the hydrodynamic drag force that opposes the displacement of the vessel, the total counter rotating mass relative to each pair of masses $m/2$ and the centrifugal force applied to each mass $m/2$, respectively. $r$, $\theta$, and $\dot{\theta}$ are the rotation radius of $m/2$, the rotation angle of the same radius, and the corresponding angular velocity, respectively. The scheme shown in Fig. 1 can be further simplified as illustrated in Fig. 2: the system is reduced to a

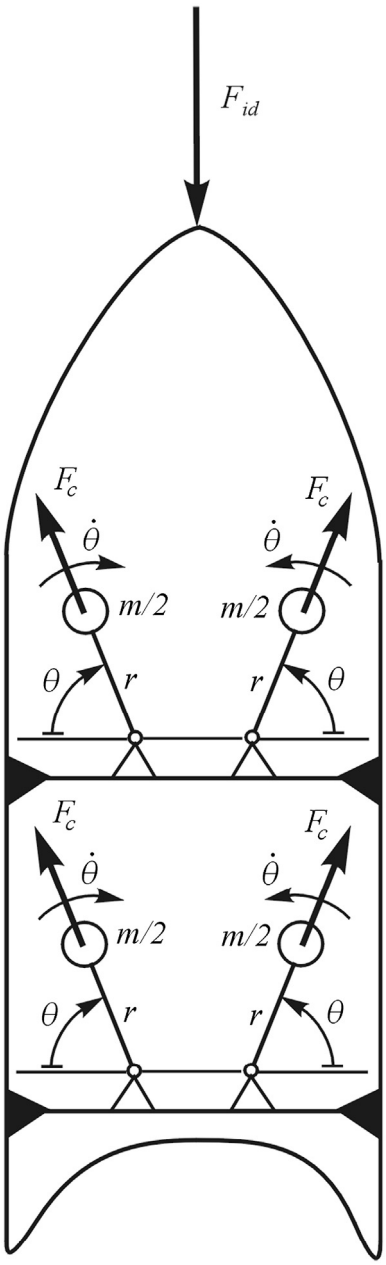


Fig. 1. Kinematic scheme of the propulsion system equipped with two pairs of counter rotating masses (Muscia, 2015a).

Please cite this article in press as: Muscia, R., Study of a vibrating propulsion system for marine vessels: Evaluation of the efficiency for a boat 13 m long, International Journal of Naval Architecture and Ocean Engineering (2016), http://dx.doi.org/10.1016/j.ijnaoe.2016.09.011

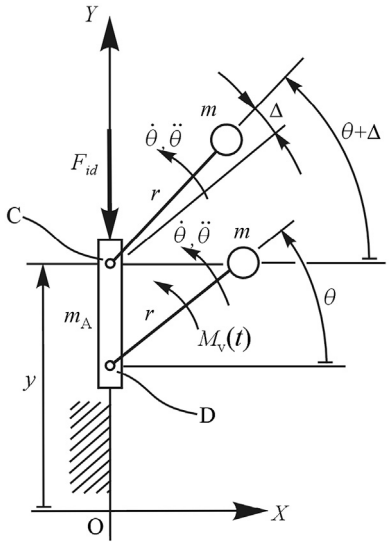


Fig. 2. Simplified kinematic scheme based on sliding fit of the propulsion system equipped with two rotating masses.

slider that oscillates along the axis *Y*. In order to obtain a dynamically equivalent system to that illustrated in Fig. 1, the counter rotating masses are hinged on this slider. In this way, one can write the motion equations of the system with greater ease. The two masses $m$ indicated in Fig. 2 are hinged at C and D, rotate with the same angular speed $\dot{\theta}$, and in general are out of phase by an angle $\Delta$. The degrees of freedom of the system are two: the displacement $y$ of the vessel and the rotation angle $\theta$ relative to the two cranks $r$. In Muscia (2015c), the two motion equations relative to $y$ and $\theta$

$$(2m+m_A)\ddot{y}+mr\left[\ddot{\theta}\cos\theta+\ddot{\theta}\cos(\theta+\Delta)-\dot{\theta}^2\sin\theta-\dot{\theta}^2\sin(\theta+\Delta)\right]=-F_{id}, \quad (1)$$

$$mr\left[\ddot{y}(\cos\theta+\cos(\theta+\Delta))+2r\ddot{\theta}\right]=M_v(t) \quad (2)$$

have been obtained by using Lagrange's equations. With reference to the scheme shown in Fig. 2, in Eqs. (1) and (2) $m_A$, $M_v(t)$, and $\ddot{\theta}$ represent the total mass of the system except the revolving one $m$, the moment applied in order to rotate the masses $m$, and the relative angular acceleration, respectively. If we fix a certain law $\theta(t)$ by which the masses $m$ rotate, we remove the rotation degree of freedom $\theta$ of the system. Therefore Eq. (1) is the only motion equation that has to be integrated to obtain $y(t)$. $y(t)$ represents the displacement of the vessel along the axis *Y* when the masses $m$ rotate with the angular speed $\dot{\theta}$ and the hull is subject to a hydrodynamic drag force $F_{id}$. Consequently, as soon as the law $\theta(t)$ is settled (it is known *a priori*) we compute $\dot{\theta}(t)$ and $\ddot{\theta}(t)$. Subsequently, based on the knowledge of the curve $F_{id}[\dot{y}(t)]$, i.e. the variation of the hydrodynamic drag force changes versus the velocity $\dot{y}(t)$, we perform the numerical integration of Eq. (1) and obtain the displacement $y(t)$ of the vessel. When $y(t)$ has been evaluated, we also know the velocity $\dot{y}(t)$ and the acceleration $\ddot{y}(t)$. Therefore, by Eq. (2) we calculate the moment $M_v(t)$ that has to be applied to the cranks $r$ to generate the displacement $y(t)$. At the current state of the research, the curve $F_{id}[\dot{y}(t)]$ has been drawn by i) fluid dynamic simulations, ii) semi-empirical methods (e.g.: Compton, 1986), and iii) correlations between experimental tests on scale models and the real system (see for example Di Ubaldo, 2010). The fluid dynamic simulations have been used primarily to evaluate $F_{id}[\dot{y}(t)]$ during the backward motion of the hull, when $\dot{y}(t)<0$. Fig. 3 shows an example relative to a curve $F_{id}[\dot{y}(t)]$ associated with a vessel whose length is approximately equal to 13 m. Fig. 4 illustrates the moment $M_v(t)$ that has to be applied between 20.0 and 20.1 s to the cranks $r$ of a vessel model whose length is approximately equal to 1.7, with $m_A = 20$ kg, $m = 2$ kg, $\Delta = 0°$, $\dot{\theta} = 235.6$ rad/s (=2250 rpm). This model covers 38 m in 40 s. In Fig. 5 an example of functions $\theta(t)$, $\dot{\theta}(t)$, and $\ddot{\theta}(t)$ that describe a startup transient, a stationary working, and a stop transient is reported.

### 2.1. Utilization of elliptical gears to increase the thrust applied to the vessel

A previous study (Muscia, 2015c) shows that it is possible to significantly increase the displacement of a hull if the rotation speed $\dot{\theta}(t)$ of each crank $r$ has a periodic impulsive trend during each revolution. Concerning this, from an engineering point of view, we can conceive a working system by considering a mesh of two elliptical gears. With reference to a uniform circular motion of a shaft on which an elliptical toothed wheel is keyed, we obtain an impulsive periodic motion of the driven shaft that is connected to the previous one by another elliptical cogwheel. The cranks $r$ that rotate the masses $m$ are keyed to the driven shaft. Therefore, each revolution of the driving shaft that rotates with constant angular velocity $\dot{\theta}$ corresponds to a revolution of the driven shaft with an angular velocity $\dot{\theta}_v(t)$ characterized by a periodic impulsive trend. In Fig. 6 an example of the function $\dot{\theta}_v(t)$ is illustrated. Fig. 7 shows a scheme of the mesh relative to the elliptical toothed wheels. In this figure the mesh of the cylindrical gears that simultaneously rotate the two cranks $r$ is also indicated. Therefore, both these cranks rotate with angular velocity $\dot{\theta}_v(t)$. In Fig. 7, $\mathscr{C}_D$, $\mathscr{C}_O$, and $\mathscr{C}_C$ represent the pitch circles of the driving, idle, and driven toothed wheels, respectively. These gears rotate the masses $m$. $\mathscr{C}_V$ and $\mathscr{C}_m$ are the pitch ellipses

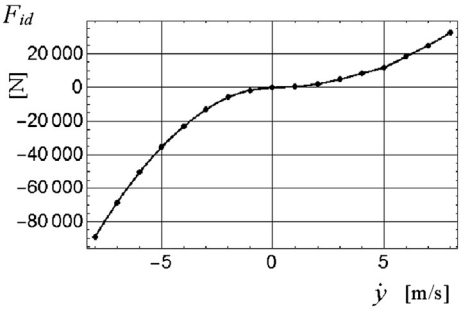


Fig. 3. An example of hydrodynamic drag force $F_{id}$ versus $\dot{y}$ for a vessel model 13 m long obtained by fluid dynamics simulations.

Please cite this article in press as: Muscia, R., Study of a vibrating propulsion system for marine vessels: Evaluation of the efficiency for a boat 13 m long, International Journal of Naval Architecture and Ocean Engineering (2016), http://dx.doi.org/10.1016/j.ijnaoe.2016.09.011

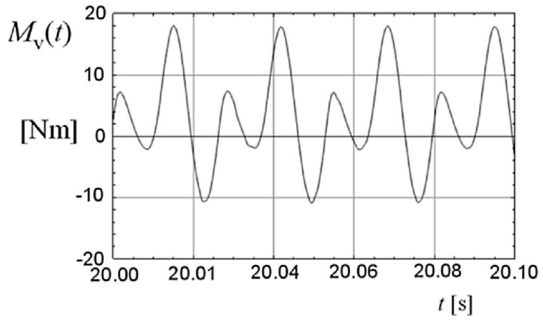


Fig. 4. Moment $M_v(t)$ versus $20.0 \leq t \leq 20.1$ applied to the cranks $r$ of a vessel model 1.7 m long with constant angular velocity $\dot{\theta}$.

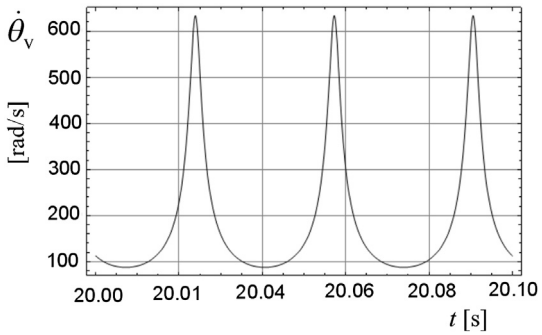


Fig. 6. Angular velocity $\dot{\theta}_v(t)$ of the masses $m$ when elliptical gears are used.

of the elliptical gears meshed. $\mathscr{C}_m$ is relative to the driving elliptical wheel, $\mathscr{C}_V$ refers to the driven elliptical wheel. This wheel is integral to the shaft on which the driving cylindrical wheel denoted by the pitch circle $\mathscr{C}_D$ is keyed. The driving cylindrical wheel $\mathscr{C}_D$ rotates with an angular speed $\dot{\theta}_v(t)$ similar to that illustrated in Fig. 6.

### 2.2. Evaluation of the propulsive efficiency

The calculation of the propulsive efficiency of the system can be performed by considering the ratio between two average powers. These powers are properly evaluated with reference to a certain interval of time relative to a stationary working of the propulsion device. In relation to the time interval to calculate these powers, we can consider the trends of the speed $\dot{y}(t)$ and the hydrodynamic drag force $F_{id}(\dot{y}(t))$ of the vessel between two successive instants $t_a$ and $t_b$. $\dot{y}(t)$ is obtained by integrating the motion equation after fixing $\theta(t)$,$\dot{\theta}(t)$, and $\ddot{\theta}(t)$. In order to define a stationary state operation, by using elliptical cogwheels, we assume $\dot{\theta}(t) = \dot{\theta}_v(t)$ and certain values $t_a$ and $t_b$ (for example, with reference to Fig. 6, we can assume $t_a = 20.0$ s and $t_b = 20.1$ s). The value of $F_{id}[\dot{y}(t)]$ at the instant $t_a \leq t \leq t_b$ is obtained by using the curve $F_{id}(\dot{y})$ ($\dot{y}(t)$ is known from the integration of the motion equation of the system). $F_{id}(\dot{y})$ is drawn by fluid dynamic simulations and/or analytical/experimental models (see for example the curve $F_{id}(\dot{y})$ shown in Fig. 3). In accordance with the principle of conservation of energy applied to the system shown in Fig. 2, we can obtain a relationship which provides the moment $M_m(t)$ that has to be applied to the driving

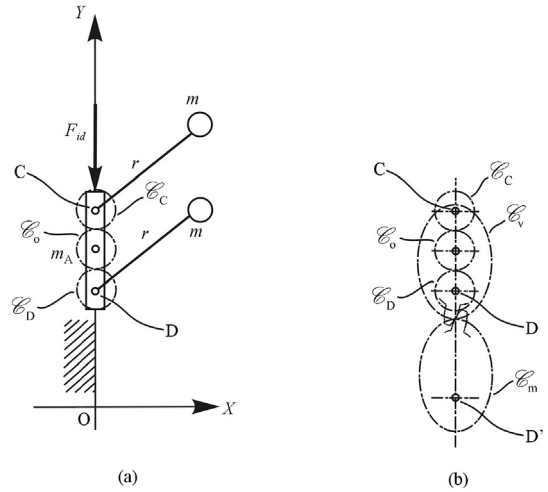


Fig. 7. (a) Train of circular gears with idle wheel to rotate and time the rotating masses $m$ and (b) functioning of the same train gears by unilobe elliptical spur gears (Muscia, 2015a,b,c).

elliptical cogwheel which rotates the counter rotating masses (Muscia, 2015c):

$$M_m(t) = \frac{m_{tot}\dot{y}(t)\ddot{y}(t) + F_{id}(t)\dot{y}(t)}{\dot{\theta}_m}. \quad (3)$$

Fig. 7b shows this cogwheel by its pitch ellipse $\mathscr{C}_m$. $M_m(t)$ depends on the speed $\dot{y}(t)$, the acceleration $\ddot{y}(t)$, $F_{id}(t)$, and the angular velocity $\dot{\theta}_m$ of the above-mentioned cogwheel. Eq. (3) is true when $\dot{\theta}_m$ is constant, i.e. when the propulsion system is operating in a steady state. This condition is simulated by assuming $\dot{\theta}_m$ equal to the value $\dot{\theta}(t)$ = cost indicated, for

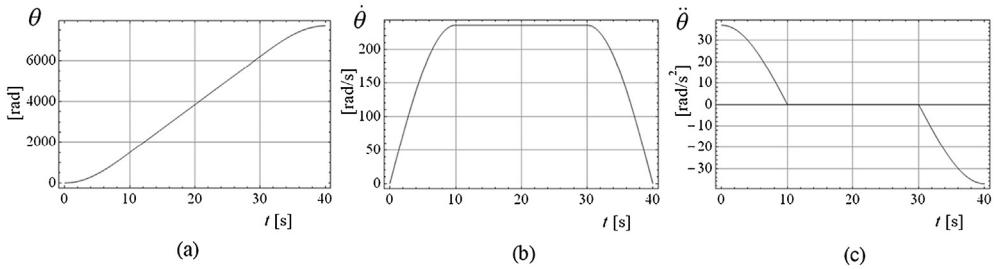


Fig. 5. An example of (a) rotation $\theta(t)$, (b) angular velocity $\dot{\theta}(t)$, and (c) angular acceleration $\ddot{\theta}(t)$ versus time relative to the crank $r$ (Muscia, 2015).

Please cite this article in press as: Muscia, R., Study of a vibrating propulsion system for marine vessels: Evaluation of the efficiency for a boat 13 m long, International Journal of Naval Architecture and Ocean Engineering (2016), http://dx.doi.org/10.1016/j.ijnaoe.2016.09.011

example, in Fig. 5b (domain of $\dot{\theta}(t)$: from 10 s to 30 s). The constant value $\dot{\theta}_m$ in that range corresponds to a periodic behaviour of $\dot{\theta}_v(t)$ caused by the mesh of the two elliptical cogwheels (see Fig. 6). Fig. 8 illustrates an example of the trend of moment $M_m(t)$ between the instants $t_a$ and $t_b$ to which the graphs $\dot{y}(t)$ and $F_{id}(t)$ reported in Fig. 9 refer. We note that in the steady state ($\dot{\theta}_m$=cost) $\dot{y}(t)$, $F_{id}(t)$, and $M_m(t)$ are periodic functions. In Eq. (3), $m_{tot}$ represents the total mass of the vessel and the counter rotating masses. Therefore, with reference to the scheme shown in Fig. 2, is

$$m_{tot} = 2m + m_A. \tag{4}$$

*2.2.1. Definition of the efficiency*

The propulsive efficiency can be calculated with reference to a time interval where the driving elliptical cogwheel rotates with an angular velocity $\dot{\theta}_m$ = const. For example, by observing Fig. 8, the interval is defined by the instants $t_a$ and $t_b$. When $\dot{\theta}_m$ = cost, the computation of two powers whose ratio provides the propulsive efficiency $\eta$ is simple. In this case $\eta$ is given by the following expression.

$$\eta = \frac{P_{md}}{P_{mav}}, \tag{5}$$

where $P_{md}$ is the average power that the system absorbs to go forward along a predetermined direction. $P_{mav}$ represents the average power furnished to the driving elliptical cogwheel in the time interval from $t_a$ to $t_b$ (it is the power supplied by the engine that drives the propulsion device, assuming a mechanical efficiency of the propulsion device equal to 1). $P_{md}$ and $P_{mav}$ are calculated with reference to the relative instantaneous powers $P_d(t)$ and $P_{av}(t)$ in the above-mentioned interval:

$$P_{mav} = \frac{1}{t_b - t_a}\int_{t_a}^{t_b} P_{av}(t)\mathrm{d}t, \tag{6}$$

$$P_{md} = \frac{1}{k}\sum_{i=1}^{k}\left(\frac{1}{t_{bi} - t_{ai}}\int_{t_{ai}}^{t_{bi}} P_d(t)\mathrm{d}t\right)_i. \tag{7}$$

Regarding Eq. (7), we observe that $P_{md}$ is obtained by computing the arithmetic mean of $k$ average powers in the range whose extremes are $t_a$ and $t_b$. Each of these powers is the average power calculated in the generic sub interval $[t_{ai},t_{bi}]$ where $\dot{y}(t)$ is positive, i.e. when the vessel moves only forward (not backward). In Fig. 9 the four intervals $[t_{ai},t_{bi}]$ ($i$ = 1, 2, …, 4) where $\dot{y}(t) > 0$ are shown. Therefore, the instantaneous power $P_d(t)$ is actually the one that is only used to cause the forward motion of the vessel. $P_d(t)$ is given by the following relationship

$$P_d(t) = F_{id}[\dot{y}(t)]\dot{y}(t). \tag{8}$$

$P_{av}(t)$ is expressed as

$$P_{av}(t) = M_m(t)\dot{\theta}_m. \tag{9}$$

$\dot{y}(t)$, $M_m(t)$, and $F_{id}[\dot{y}(t)] = F_{id}(t)$ are known versus $t$ as soon as the motion equation (1) of the system has been integrated. Consequently, we can compute $P_d(t)$, $P_{av}(t)$, $P_{md}$, $P_{mav}$, and $\eta$.

*2.3. Practical application and critical issue of the proposed system*

The propulsion system discussed in the previous sections is still in progress and the present work aims to evaluate its potential future applications. From the physical point of view the developed models indicate that the system should work, i.e. it should be able to push the vessel with a certain efficiency. This efficiency, as it will be shown in Section 3, depends a lot on the total mass $m_{tot}$ of the system and the ratio between the mass $m_A$ of the vessel and the counter rotating mass $m$. Moreover, as well the curve of hydrodynamic drag force $F_{id}$ versus the speed $\dot{y}$ of the boat is crucial to achieving a high propulsive efficiency $\eta$. In this regard, we usually note that the greater the value of $F_{id}$ during the backward motion with respect to the forward one is, the higher $\eta$ is, velocity $\dot{y}$ being equal. Furthermore, although high forward average velocities often correspond to a higher propulsive efficiency $\eta$, when these velocities are too high, $\eta$ tends to decrease. We can observe that a set of parameters that maximizes the vessel speed and its propulsive efficiency certainly exists. In any case, as it will be shown in Section 3, there are suggestions

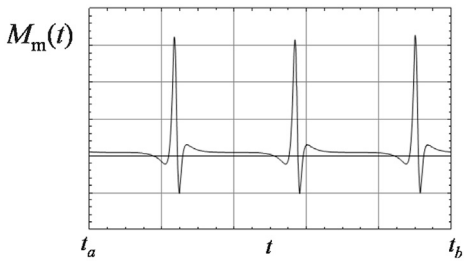


Fig. 8. Torque $M_m(t)$ applied to the driving elliptical wheel versus $t_a \le t \le t_b$.

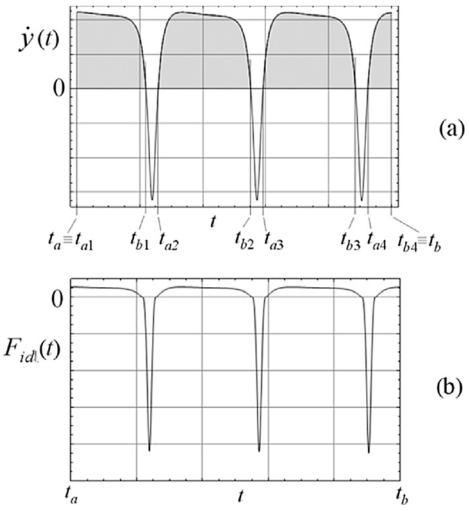


Fig. 9. (a) Velocity$\dot{y}(t)$ and (b) hydrodynamic drag force $F_{id}(t)$ versus time $t_a \le t \le t_b$ of the vessel during a stationary working of the propulsion device.

Please cite this article in press as: Muscia, R., Study of a vibrating propulsion system for marine vessels: Evaluation of the efficiency for a boat 13 m long, International Journal of Naval Architecture and Ocean Engineering (2016), http://dx.doi.org/10.1016/j.ijnaoe.2016.09.011

that can allow a further development of this research. As a matter of fact, even though the forward velocities are still relatively small and only in some cases the propulsive efficiency $\eta$ is acceptable (i.e., $\eta$ is comparable with that of the propeller propulsion), there are possibilities that can still be explored. We observe that results of the simulations can improve, by always considering the practical aspects of the problem. The sterns shaping characterized by a high hydrodynamic drag force $F_{id}$ during the backward motion and hulls with low $F_{id}$ during the forward motion, combined with a reduction of the vessel mass are the elements that allow the performance of the propulsion system to significantly increase. Other issues to consider regard i) the design of appropriate elliptical cogwheels able to generate impulsive thrusts and ii) a suitable choice of the rolling or fluid dynamic bearings (similar to the crankshaft bearings of the internal combustion engines). These bearings support the various shafts on which the toothed wheels are keyed (see for example Fig. 7). The forces, however high, can be supported by a suitable dimensioning of the various mechanical parts of the propulsion system, at least in relation to a first prototype manufacturing. The vibrations transmitted to the hull, in the present state of the study, have not been analysed yet. However, if for example the counter rotating masses rotate at 3000 rpm, the excitation frequency of the first order will be equal to 50 Hz. In relation to this frequency value and those relative to the higher harmonics, in order to reduce the problems of transmission of vibrations, vibration isolators could be considered.

## 3. Application to a real boat

The physical mathematical model illustrated in the previous sections has been applied to a vessel of which the length is equal to little more than 13 m. This vessel has already been manufactured and is currently equipped with a propeller propulsion system. The CAD model of the vessel (Quondamatteo, 2011) has been suitably modified so as to be able to perform fluid dynamics simulations. The aim of these simulations was the evaluation of the hydrodynamic drag force during the backward and forward motion of the vessel. Fig. 10 shows the simplified CAD model used to obtain the curves of the hydrodynamic drag force versus the velocity. In this figure the possible overall dimensions of the propulsion system equipped with the counter rotating masses installed on board the vessel are also indicated (see the parallelepiped dimensioned). For example, the dimensions refer to a device equipped with twenty counter rotating masses. The values of these masses have been obtained by splitting the pairs of masses $m$ illustrated in Fig. 2 into small masses. Many fluid dynamics simulations were performed by always considering a vessel draught equal to 1000 mm, in a displacement hull condition. In addition to the CAD model shown in Fig. 10, the model shown in Fig. 11 was also used. This new model shows a modified stern. It represents an attempt to obtain a curve $F_{id}(\dot{y})$ of which the values during the backward motion are noticeably higher than those during the forward motion. In this way the forward thrust can be increased. The modified stern model has three

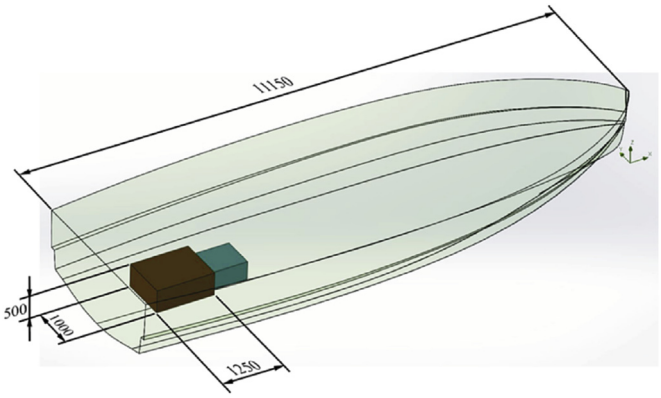


Fig. 10. A basic vessel CAD model used to perform the fluid dynamics simulations and possible overall dimensions of the counter rotating masses propulsion device.

empty helical cavities. By fluid dynamics simulations (Valeri, 2015) it has been proved that this configuration of the stern enables one to increase and decrease the hydrodynamic drag force when the vessel moves backward ($\dot{y}(t) < 0$) and forward ($\dot{y}(t) > 0$), respectively. This idea has been developed by considering that a vortical field always causes a dissipation of energy greater than the case in which the vorticity is absent. Consequently, a vorticity by the helical cavities has deliberately been induced inside the stern. For example, in Fig. 12a and b the flow streams that show this vorticity are illustrated, during the backward and forward hull motion, respectively. By observing these flow streams, we detect a greater vorticity during the backward motion with respect to the forward one. Therefore during the backward motion $F_{id}(\dot{y})$ increases and we also obtain a reduction of $F_{id}(\dot{y})$ when $\dot{y}(t) > 0$. In Fig. 12c and d, the flow streams relative to the same hull are illustrated but, in this case, the stern is flat. If we compare the figures, in the case of the modified stern a considerable slowdown of the fluid velocity is noticed. This fact causes an overall increase in the average forward velocity of the vessel. In the following sections these results will be quantitatively illustrated and, in particular, the propulsive efficiency will be evaluated versus various curves $F_{id}(\dot{y})$ and masses $m_A$ and $m$. Table 1 summarizes the main features of the boat considered to perform the above-mentioned simulations.

### 3.1. Evaluation of the curves $F_{id}(\dot{y})$

Many evaluations of the hydrodynamic drag force $F_{id}$ versus different velocities of the vessel have been performed. The software Flow Simulation integrated with SolidWorks solid modeller was used (Flow Simulation, SolidWoks, Dassault Systèmes, 2015). In Fig. 13 the results obtained by 32 fluid dynamics simulations are reported (see the points in the graphics): 16 simulations were relative to the hull with a flat stern (see the curve $F_{id0}$ and Figs. 10, and 12c,d) and the other 16 concerned the hull with the stern shaped by helical cavities (see Figs. 11 and 12a,b). The velocities $\dot{y}$ considered change from −8 m/s to +8 m/s. Higher speeds have not been

Please cite this article in press as: Muscia, R., Study of a vibrating propulsion system for marine vessels: Evaluation of the efficiency for a boat 13 m long, International Journal of Naval Architecture and Ocean Engineering (2016), http://dx.doi.org/10.1016/j.ijnaoe.2016.09.011

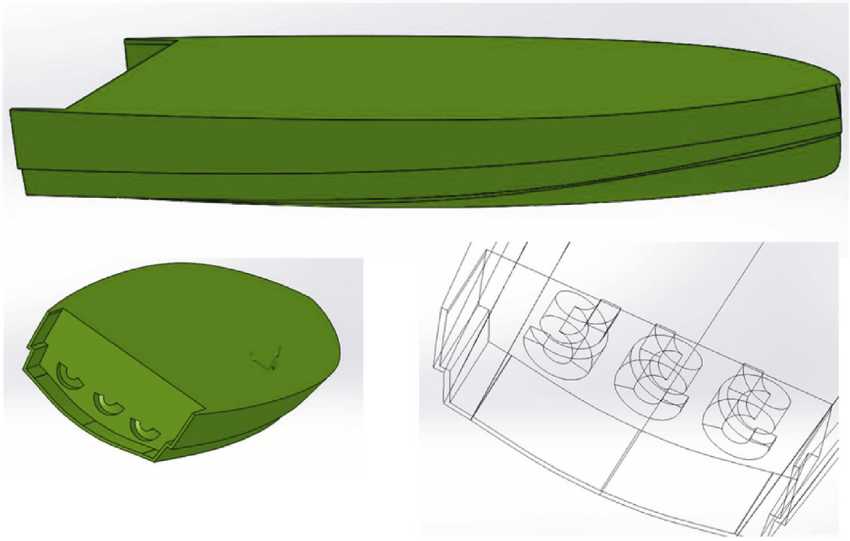

Fig. 11. Three CAD images of the model of the vessel model with stern modified to increase the hydrodynamic drag force during the backward motion of the hull.

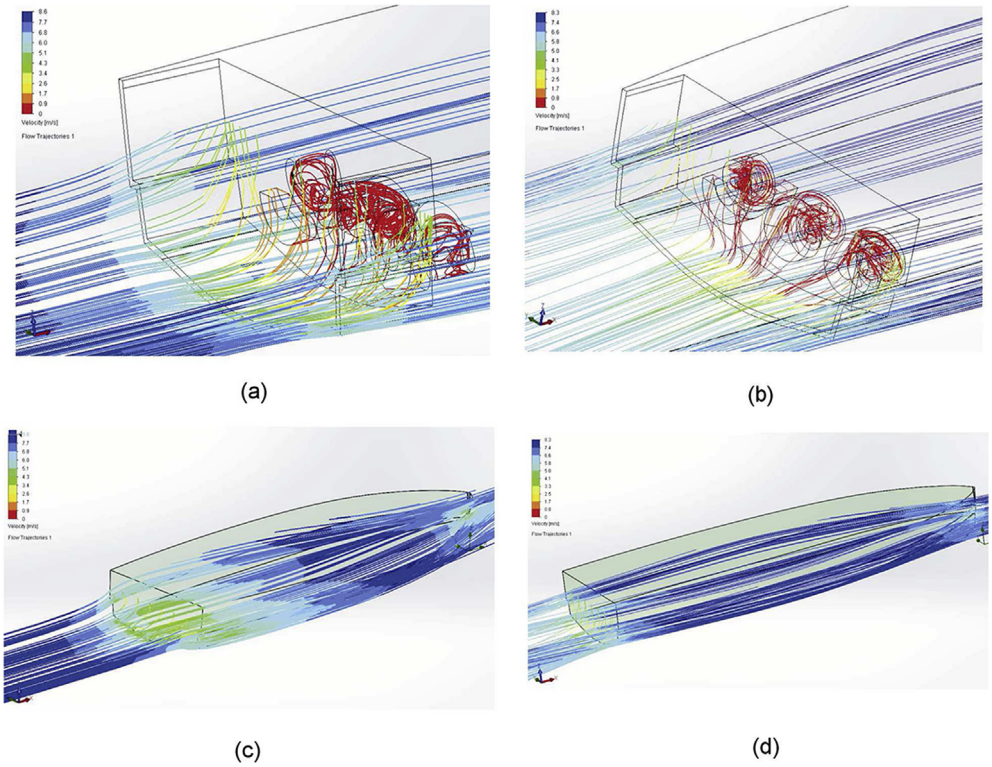


Fig. 12. Flux lines in the stern zone with helicoidal cavities during the (a) backward and (b) forward motion of the hull; flux lines during the (c) backward and (d) forward motion of the hull with flat stern (not modified).

considered because, for simplicity, the fluid dynamic simulations were performed with reference to a total displacement hull, condition which usually occurs when the velocities of the vessel are small.

By observing the curves obtained by the spline interpolation of each set of 17 points relative to the 17 values of $\dot{y}$, we note that the absolute values of $F_{id}$ during the backward motion are significantly higher in the case of the stern with the helical cavities with respect to those relative to the flat stern. At the same time, if we consider the modified stern, during the forward motion $F_{id}$ is smaller than that associated with the flat stern. Therefore, as we will illustrate in the following, by the modified stern, in general we obtain a greater mean forward velocity. Since the shape of the backward motion $F_{id}(\dot{y})$ curve is particularly important in order to maximize the propulsive efficiency and the forward speed of the vessel, the motion Equation (1) has been integrated by considering various $F_{id}(\dot{y})$ curves. These curves have been obtained by using those

Please cite this article in press as: Muscia, R., Study of a vibrating propulsion system for marine vessels: Evaluation of the efficiency for a boat 13 m long, International Journal of Naval Architecture and Ocean Engineering (2016), http://dx.doi.org/10.1016/j.ijnaoe.2016.09.011

Table 1
Main characteristics of the case study vessel.

| | |
|---|---|
| Length overall | 13.3 m |
| Length waterline | 13.10 m |
| Width waterline | 3.45 m |
| Maximum width | 3.89 m |
| Draught | 1.2 m |
| Hull | Semi-displacement hull |
| Cruising speed | 20 knots (full load) |
| Number of engines | 2 |
| Number of propellers | 2 |
| Number of transmission shafts | 2 |
| Number of manoeuvre propellers | 1 |
| Displacement | 11,000 kg |

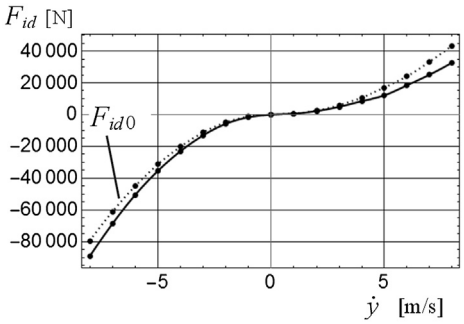


Fig. 13. Comparison between the hydrodynamic drag force $F_{id}$ relative the stern modified (continuous line) and not modified ($F_{id0}$ dotted line).

illustrated in Fig. 13. In Fig. 14 three examples of such curves are shown. In the first case we assume to be able to shape the stern and/or the hull in order to obtain a backward motion$F_{id}(\dot{y})$ linearly scaled by a constant coefficient (see the curve $F_{id1}$). The curve $F_{id2}$ illustrated in Fig. 14 was obtained by multiplying the values of the curve $F_{id1}$ by a constant equal to 1.2. The other curve $F_{id3}$ was drawn by multiplying the values of the curve $F_{id1}$ by a non-linear function of $\dot{y}$. For $\dot{y}>0$, the function $F_{id}(\dot{y})$ is always that relative to the stern shaped by the helical cavities (see the curve $F_{id1}$). Other

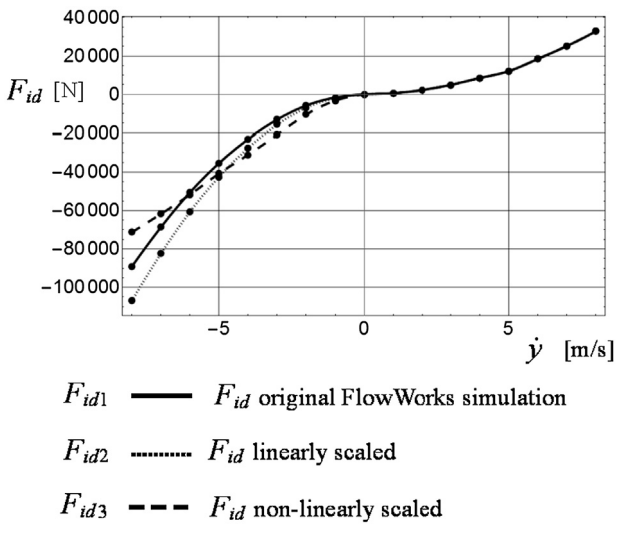


Fig. 14. Three example of hydrodynamic drag force $F_{id}(\dot{y})$ modification in the velocity domain $\dot{y}<0$.

curves $F_{id}(\dot{y})$ have been obtained by semi-empirical methods (e.g.: Compton, 1986) and correlations between experimental tests on scale models and the real system (see Flavio Di Ubaldo, 2010). In relation to the above-mentioned methods, the values of $F_{id}$ versus $\dot{y}<0$ could not be obtained or were not available. Consequently, these curves $F_{id}(\dot{y})$ have been completed in the domain $\dot{y}<0$ by using those obtained by the fluid dynamics simulations.

In Fig. 15 an example of these "mixed" curves is reported (see Fig. 15a and the curve $F_{id}(\dot{y})$ denoted by $F_{id4}$). Another kind of curve was obtained by using the ratio between the values of $F_{id}$ computed by the fluid dynamics simulations and semi-empirical/correlation methods. For each value of $\dot{y}>0$ the above-mentioned ratio was calculated. Therefore, each value of $F_{id}(\dot{y})$ relative to the domain $\dot{y}<0$ obtained by the fluid dynamics simulations (see the curve $F_{id}(\dot{y})$ versus $\dot{y}<0$ in Fig. 15a) and associated with the same value $|\dot{y}|$, was multiplied by the ratio previously mentioned. In this way the curve $F_{id}(\dot{y})$ relative to the backward motion obtained by the simulation has been non-linearly scaled with reference to the same ratio which is defined between the two forward motion curves $F_{id}$ (one is obtained by the simulation and the other by semi-empirical/correlation methods). In this way we have reasonably tried to correct the simulation data in relation to those obtained by semi-empirical/correlation that could be more accurate, but not available for the backward motion. Fig. 15b shows the curve $F_{id5}$ obtained by using the procedure illustrated. Another kind of curve $F_{id}(\dot{y})$ has been obtained by combining the backward motion curve $F_{id2}$ and the forward motion one $F_{id4}$. In Fig. 15b the curve drawn is denoted by $F_{id6}$. Finally, a further curve $F_{id7}$ was considered (see Fig. 15b). $F_{id7}$ has been obtained by combining the curves $F_{id3}$ and $F_{id4}$ relative to $\dot{y}<0$ and $\dot{y}>0$, respectively.

### 3.2. Integration of the motion equation: results obtained

The integration of the motion equation of the system (1) was carried out by fixing *a priori* the rotation $\theta_m(t)$, the angular speed $\dot{\theta}_m(t)$, and acceleration $\ddot{\theta}_m(t)$ of the driving elliptical cogwheel. Fig. 16 illustrates a simple trend of the above-mentioned functions: we observe a startup transient, a stationary working (constant angular velocity $\dot{\theta}_m = 3000$ rpm), and a stop transient. The functions illustrated in Fig. 16 were used for most of the simulations. As soon as $\theta_m(t)$, $\dot{\theta}_m(t)$, and $\ddot{\theta}_m(t)$ are fixed, by applying the kinematics of the elliptical cogwheels (Kowalczyk, Urbanek, 2003) the corresponding rotation$\theta_v(t)$, angular velocity $\dot{\theta}_v(t)$, and acceleration $\ddot{\theta}_v(t)$ of the driven elliptical cogwheel are obtained. Fig. 17 shows these functions. The procedure of calculation to evaluate the angular speed of the elliptical toothed wheel driven by the driving wheel is illustrated in Muscia, 2015c. Therefore, $\theta_v(t)$, $\dot{\theta}_v(t)$, and $\ddot{\theta}_v(t)$ are the functions $\theta(t)$, $\dot{\theta}(t)$, and $\ddot{\theta}(t)$ that have been used to integrate the motion equation (1). Table 2 reports the values of the masses $m_A$ and $m$, the values of the radius $r$, and the angle $\Delta$ used to perform some integrations of Eq. (1). These values enable us to compute certain performances of the propulsion system. In relation to such values, the analysis can

Please cite this article in press as: Muscia, R., Study of a vibrating propulsion system for marine vessels: Evaluation of the efficiency for a boat 13 m long, International Journal of Naval Architecture and Ocean Engineering (2016), http://dx.doi.org/10.1016/j.ijnaoe.2016.09.011

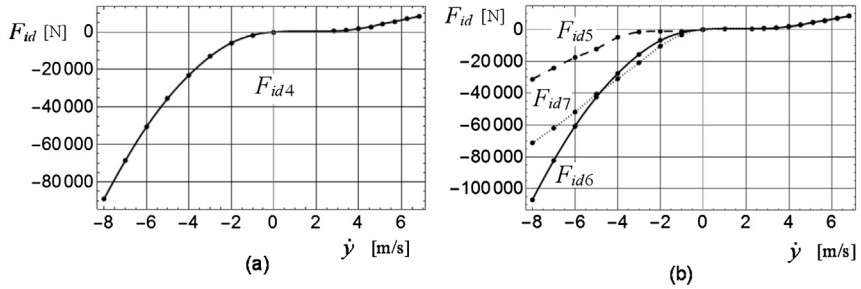


Fig. 15. Hydrodynamic drag force $F_{id4}$ obtained by (a) fluid dynamics simulations ($\dot{y}$<0) and by experimental models ($\dot{y}$>0), (b) various curves $F_{id}$.

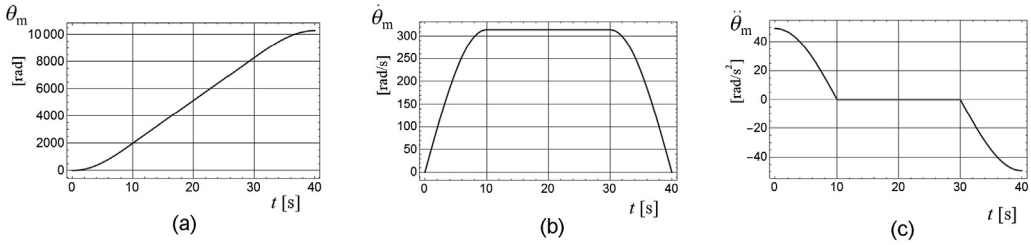


Fig. 16. (a) Rotation $\theta_m(t)$, (b) angular velocity $\dot{\theta}_m(t)$, and (c) angular acceleration.$\ddot{\theta}_m(t)$ versus time of the driving elliptical gear of the propulsion system.

definitely be performed in depth by a systematic research aimed at identifying which are the values most advantageous. For example, we can formulate a multiobjective constrained optimization problem where the two main objective functions could be the propulsive efficiency and the distance covered by the vessel, both to be maximized (with reference to a steady state working). The value of $\Delta$ equal to zero has enabled us to obtain the best results (at least in relation to the simulations performed). Concerning the mass $m$ equal to 500 kg, it is expected to split $m$ into smaller masses so as to reduce the value of the centrifugal force applied to the shafts and the relative bearings of the propulsion device. For example, by considering a splitting of $m$ by ten mass $m_p = 50$ kg and ten mechanisms of the kind illustrated in Figs. 1 and 2 and installed in the hull, it is possible to reduce the peaks of the magnitude $F_r$ of the centrifugal and tangential forces that stress the system. $F_r$ is calculated as a function of $\dot{\theta}_v(t)$ and $\ddot{\theta}_v(t)$. Fig. 18 shows $F_r$ versus time from 15.0 to 15.1 s, during the phase of steady functioning (see the curve $\dot{\theta}_m(t)$ in Fig. 16b) with reference to the mass $m_p = 50$ kg. From an engineering point of view, the overall dimensions of such a system may be those indicated in Fig. 10 (see the parallelepiped dimensioned). The maximum values of $F_r$ are high, but they are peak values: their duration is extremely short (it is a situation similar to that which occurs with the crankshaft main bearings of an internal combustion engine). Therefore, it is possible to design shafts and bearings able to endure these forces. Hydrodynamic bearings, similar to those of the crankshafts or even rolling bearings could be used. In a specific case, a suitable rolling bearing could be the one shown in Fig. 19 (a toroidal type bearing characterized by high performance). A distribution of the mass $m$ into smaller masses $m_p$ surely reduces the size of the bearings but, the performance of the propulsion system being equal, it is necessary to increase the number of masses $m_p$. Fig. 20 illustrates an example of the results obtained by integrating the equation of motion (1) of the system. This figure reports the displacement $y(t)$, velocity $\dot{y}(t)$, and acceleration $\ddot{y}(t)$ of the vessel with reference to the angular speed of the driving elliptical cogwheel shown in Fig. 16. We can observe that the responses indicated in Fig. 20 have been obtained by using the hydrodynamic drag curve

Table 2
Some values of the masses and crank radius $r$ used to simulate the dynamic behaviour of the vessel study.

| | |
|---|---|
| $m$ | 500 kg |
| $m_A$ | 5000, 6000, 7000, 8000, 11,000 kg |
| $r$ | 0.1 m |
| $\Delta$ | 0 Degrees |

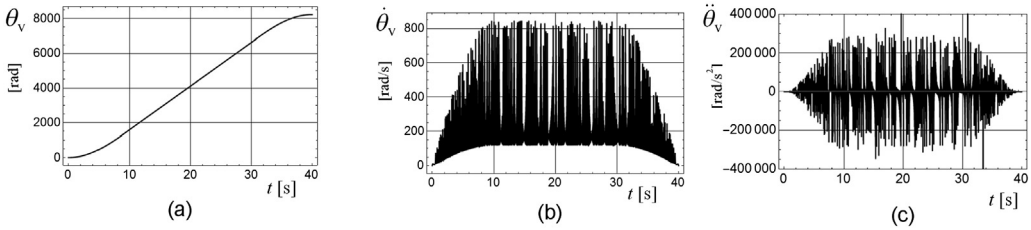


Fig. 17. (a) Rotation $\theta_v(t)$, (b) angular velocity $\dot{\theta}_v(t)$, and (c) angular acceleration.$\ddot{\theta}_v(t)$ versus time for the driven elliptical gear of the propulsion system.

Please cite this article in press as: Muscia, R., Study of a vibrating propulsion system for marine vessels: Evaluation of the efficiency for a boat 13 m long, International Journal of Naval Architecture and Ocean Engineering (2016), http://dx.doi.org/10.1016/j.ijnaoe.2016.09.011

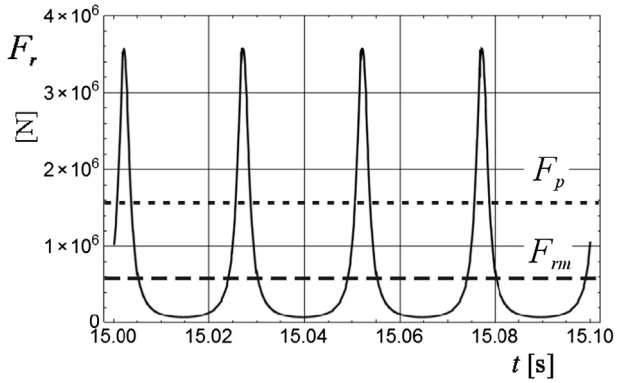


Fig. 18. Resultant force $F_r$ applied the rotating reduced masses $m_p = 50$ kg versus time during the stationary operation with $\dot{\theta}_m = 314.1$ rad/s (= 3000 rpm), mean value $F_{rm}$ and bearing equivalent load $F_p$.

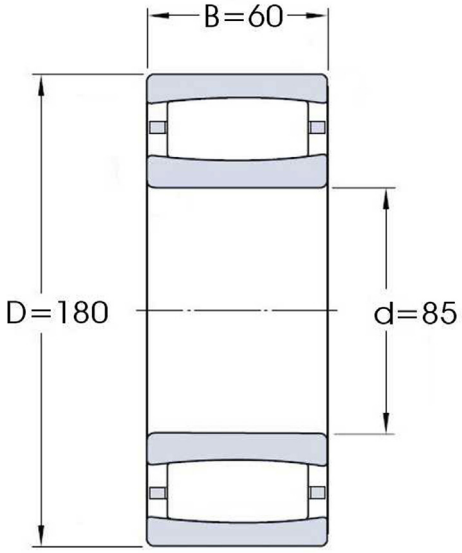


Fig. 19. Dimensions (mm) of the SKF carb toroidal roller bearing C2137 with basic load ratings dynamic and static equal to 540 and 600 KN, respectively (limiting speed 3200 rpm, mass 7.4 kg).

denoted in Table 3 by $F_{id4}$. $F_{id4}$ identifies the curve $F_{id}(\dot{y})$ shown in Fig. 15a, that is the one obtained by the fluid dynamics simulations when $\dot{y} < 0$ and by semi-empirical methods and correlations (see Di Ubaldo, 2010; Compton, 1986) when $\dot{y} > 0$. In this case it is noted that the vessel should cover about 115 m in 40 s (see $y_{40s}$ and the average speed $\dot{y}_m$ approximately equal to 3.5 m/s in Table 3). Unfortunately, the propulsive efficiency $\eta$ is rather low (it is equal to 0.11) and the average power $P_{mav}$ that the motor has to provide is approximately equal to 207 kW (see Table 3). It is also observed that this result was obtained by setting $m_A = 7000$ kg, i.e. the vessel has to be lighter than that already manufactured (of which the mass is about equal to 11,000 kg). In this regard, the results drawn through some simulations show that the propulsive efficiency $\eta$ depends heavily on the value of the vessel mass $m_A$: in general, the smaller the mass $m_A$ is, the greater $\eta$ and the steady average speed $\dot{y}_m$ are. However, with reference to the simulations performed, only in one case we obtained a relatively high efficiency ($\eta = 0.39$) relative to a not too small $\dot{y}_m$ (4.36 m/s). The parameters that have allowed us to obtain this result are reported in Table 3: extremely lightweight vessel ($m_A = 5000$ kg) and non-linear curve $F_{id}$ versus $\dot{y}$ when $\dot{y}<0$. These values allow one to increase the hydrodynamic drag force at low backward velocities (see the curve denoted by $F_{id7}$ in Fig. 15b).

### 3.3. Correlation between experiments on model and possible full scale application

The simulations performed are substantially based on the curves of the hydrodynamic drag force $F_{id}(\dot{y})$ obtained by the finite volume method (Flow Simulation, SolidWorks, Dassault Systèmes, 2015), semi-empirical methods, and correlations between experimental tests on scale models and the real system (Compton, 1986; Di Ubaldo, 2010). These approaches have some degree of approximation and introduce errors in the evaluation of the average power $P_{mav}$ and $\dot{y}_m$. Such errors can produce an appreciable effect on the computation of the propulsive efficiency $\eta$, input average power $P_{mav}$, and average speed $\dot{y}_m$. In order to assess these effects the various curves $F_{id0}$, $F_{id1}$, …, $F_{id7}$ used to integrate the equation of motion (1) were considered. However, the simulations indicate that an advantageous way to increase $\eta$ is to consider curves $F_{id}(\dot{y})$ where the values of the hydrodynamic drag force are relatively high when the backward velocities are lower (see the curve $F_{id7}$ in Fig. 15b). Furthermore in general the higher forward average speed $\dot{y}_m$ is, the lower the ratio $m_A/m$ is. Therefore, the propulsion system has higher performance when the vessel is lighter, all things being equal. In relation to this aspect, the structural solutions of the vessel should be inspired, as far as possible, by those of aeronautical kind, in order to reduce the weights and, at the same time, ensuring adequate strength from a mechanical point of view. Finally, we observe that a procedure to model favourable sterns could limit the problem of optimization of the system in two successive phases. The

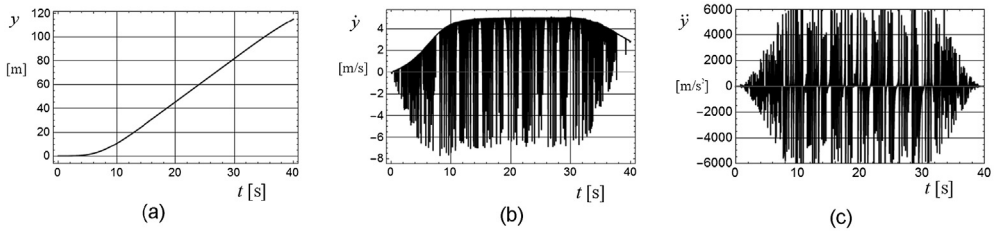


Fig. 20. (a) Displacement $y(t)$, (b) velocity $\dot{y}(t)$, and (c) acceleration $\ddot{y}(t)$ versus time for the 13 m long vessel with stern modified (see Fig. 3a and b).

Please cite this article in press as: Muscia, R., Study of a vibrating propulsion system for marine vessels: Evaluation of the efficiency for a boat 13 m long, International Journal of Naval Architecture and Ocean Engineering (2016), http://dx.doi.org/10.1016/j.ijnaoe.2016.09.011

Table 3
Parameters and results relative to some simulations.

| $F_{id}$ | $F_{id0}$ | $F_{id1}$ | $F_{id1}$ | $F_{id1}$ | $F_{id1}$ | $F_{id2}$ | $F_{id3}$ | $F_{id4}$ | $F_{id4}$ | $F_{id4}$ | $F_{id5}$ | $F_{id5}$ | $F_{id6}$ | $F_{id7}$ |
|---|---|---|---|---|---|---|---|---|---|---|---|---|---|---|
| $m$ [kg] | 500 | 500 | 500 | 500 | 500 | 500 | 500 | 500 | 500 | 500 | 500 | 500 | 500 | 500 |
| $m_A$ [kg] | 5000 | 5000 | 6000 | 7000 | 8000 | 11,000 | 5000 | 7000 | 8000 | 11,000 | 5000 | 11,000 | 5000 | 5000 |
| $\eta$ | 0.11 | 0.148 | 0.100 | 0.086 | 0.075 | 0.051 | 0.103 | 0.113 | 0.096 | 0.025 | 0.06 | 0.004 | 0.147 | **0.390*** |
| $y_{40s}$ [m] | 78.9 | 97.4 | 80.9 | 63.3 | 60.0 | 49.3 | 89.2 | 115.1 | 104.2 | 75.7 | 103.5 | 35.0 | 160.6 | 145.1 |
| $\dot{y}_m$ [m/s] | 2.43 | 3.03 | 2.52 | 1.90 | 1.90 | 1.52 | 2.70 | 3.54 | 3.22 | 2.25 | 3.22 | 0.97 | 4.91 | 4.36 |
| $P_{mav}$ [kW] | 421.3 | 367.6 | 429.0 | 256.4 | 202.5 | 144.5 | 395.2 | 206.9 | 118.2 | 94.6 | 322.8 | 174.9 | 325.4 | 95.3 |

* The highest efficiency obtained.

first phase consists in finding a reasonable curve $F_{id}(\dot{y})$ that maximizes the efficiency $\eta$ and/or the speed $\dot{y}_m$. When this curve $F_{id}(\dot{y})$ is known, we should optimize the shape of the stern so as to obtain by the fluid dynamic simulations the same $F_{id}(\dot{y})$ obtained by the previous optimization.

## 4. Conclusions

In this study we have illustrated the results obtained by numerical simulations considering a propulsion system based on counter rotating masses. The simulations were performed by using a 3D CAD model of a vessel of which the length is equal to about 13 m, with reference to a displacement hull condition. The results show that the non-conventional propulsion system still requires improvements to be competitive with respect to the traditional propeller propulsion. These improvements could make it more advantageous than the traditional screw propulsion. Lighter hull structures together with appropriate shaped sterns and bows to increase and reduce the hydrodynamic drag force during backward and forward motion represent some aspects that have to be considered in order to improve the system performances. Future developments will concern the formulation of a new propulsive model with another degree of freedom. By this new degree of freedom we will evaluate the dynamical effects on the propulsion due to the vibration isolators that have to be used to join the propulsion device to the hull. Resonance phenomena and the consequent energy transfer in the system water-hull-propulsion device will be studied.

## Acknowledgements

The author would like to thank Prof. Igor Zotti, University of Trieste, Italy and Dr. Eng. Lucio Marquardt, Cantieri Alto Adriatico, Monfalcone, Italy for their availability to furnish data and CAD models relative to the vessel case study.

## References

Belibassakis, K.A., Politis, G.K., 2013. Hydrodynamic performance of flapping wings for augmenting ship propulsion in waves. Ocean. Eng. 72, 227–240.
Chernousko, F.L., 2002. The optimum rectilinear motion of a two-mass system. Prikl. Mat. Mekh. 66 (1), 3–9.
Chernousko, F.L., 2005. The motion of a body containing a mobile internal mass. Dokl. Akad. Nauk. SSSR 405 (1), 56–60.
Chernousko, F.L., 2006. Analysis and optimization of the motion of a body controlled by means of a movable internal mass. Prikl. Mat. Mekh. 70 (6), 915–941.
Chernousko, F.L., 2008. The optimal periodic motions of a two-mass system in a resistant medium. J. Appl. Math. Mech. 72, 116–125.
Compton, R.H., 1986. Resistance of a systematic series of semiplaning transform stern hulls. Marit. Technol. 23 (4).
Di Ubaldo, F., 2010. General Design of a 13 m Motor – Yacht. Thesis. Dipartimento di Ingegneria navale, del mare e per l'ambiente, Università di Trieste.
Esfahani, J.A., Karbasian, H.R., Barati, E., 2015. Proposed kinematic model for fish-like swimming with two pitch motions. Ocean. Eng. 104, 319–328.
Fang, H., Xu, J., 2012. Dynamics of a three-module vibration-driven system with non-symmetric Coulomb's dry fiction. Multibody Syst. Dyn. 27, 455–485.
Fang, H., Xu, J., 2011. Dynamics of a mobile system with an internal acceleration-controlled mass in a resistive medium. J. Sound Vib. 330, 4002–4018.
Floc'h, F., Phoemsapthawee, S., Laurens, J.M., Leroux, J.B., 2012. Porpoising foil as a propulsions system. Ocean. Eng. 39, 53–61.
Flow Simulation, SolidWorks, 2015. Dassault Systèmes.
Guglielmini, L., Blondeaux, P., Vittori, G., 2004. A simple model of propulsive oscillating foils. Ocean. Eng. 31, 883–899.
Kowalczyk, L., Urbanek, S., 2003. The geometry and kinematics of a toothed gear of variable motion. Fibres Text. East. Eur. July, Sept. 2003 11 n. 3(42).
Li, H., Furuta, K., Chernousko, F.L., 2005. A pendulum-driven cart via internal force and static friction. In: Proceedings of the International Conference "Physics and Control", Saint Petersburg, Russia, pp. 7–15.
Li, H., Furuta, K., Chernousko, F.L., 2006. Motion generation of the Capsubot using internal force and static friction. In: Proceedings of the 45th IEEE Conference on Decision and Control, San Diego, CA, USA, pp. 6575–6580.
Muscia, R., 2015a. Evaluation of the efficiency of a vibrating propulsion system for marine vessels, Part I: physical mathematical models. In: Proceedings of the 18th International Conference on Ships and Shipping Research, Lecco, Italy, pp. 337–347.
Muscia, R., 2015b. Evaluation of the efficiency of a vibrating propulsion system for marine vessels, Part II: integration of motion equations and performances. In: Proceedings of the 18th International Conference on Ships and Shipping Research, Lecco, Italy, pp. 349–359.
Muscia, R., 2015c. Performance improvement of a vibration driven system for marine vessels. J. Multibody Syst. Dyn. (Springer). http://dx.doi.org/10.1007/s11044-015-9465-8.
Muscia, R., Sciuto, G., 2010. Analytic study of a new conceptual propulsion device for ships. Int. J. Nav. Archit. Ocean Eng. 2 (2), 75–86.
Quondamatteo, F., 2011. Confronto idrodinamico di carene per imbarcazioni da diporto. Dipartimento di Ingegneria navale, del mare e per l'ambiente, Università di Trieste. Thesis.
Shaw, S.W., 1986. On the dynamic response of a system with dry friction. J. Sound Vib. 108 (2), 305–325.
Valeri, D., 2015. Modellazione di famiglie di poppe di natanti predisposte per un sistema propulsivo senza elica: prima valutazione della resistenza idrodinamica all'avanzamento e all'arretramento. Thesis in progress. Dipartimento di Ingegneria e Architettura, Università di Trieste.
Xia, D., Chen, W., Liu, J., Wu, Zhijun, Cao, Y., 2015. The three-dimensional hydrodynamics of thunniform swimming under self-propulsion. Ocean. Eng. 110, 1–14.
Yang, L., Wiercigroch, M., Pavlovskaia, E., Yu, H., 2013. Modelling of a vibro-impact capsule system. Int. J. Mech. Sci. 66, 2–11.

Please cite this article in press as: Muscia, R., Study of a vibrating propulsion system for marine vessels: Evaluation of the efficiency for a boat 13 m long, International Journal of Naval Architecture and Ocean Engineering (2016), http://dx.doi.org/10.1016/j.ijnaoe.2016.09.011